Nerf Blaster Redesign

ME4041 Computer Graphics and CAD

April 30, 2010

Submitted By:

Michael Schulman

Greg Mann

Table of Contents

Introduction

The Nerf Longstrike CS-6 long range blaster was chosen for redesign. The blaster shoots foam darts with a reported range of 35 feet. Figure 1 shows a picture of the blaster.

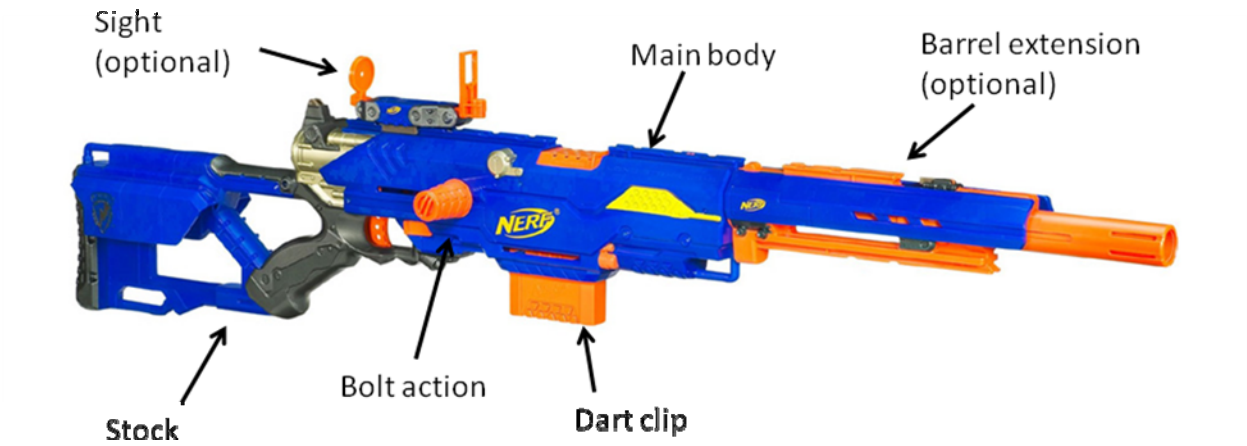

Figure 1: Longstrike CS-6 blaster

The main body houses the internal components and functional mechanisms. The blaster has a removable barrel extension and sight. The dart clip holds 6 darts, which are loaded by a bolt action. The blaster comes partially unassembled, with a stock that is inserted into the back of the blaster and locked by permanent clips internally. This blaster is rated for children ages 6 years and older, with a targeted market of boys age 10-12.

Figure 2 shows an internal view of the blaster.

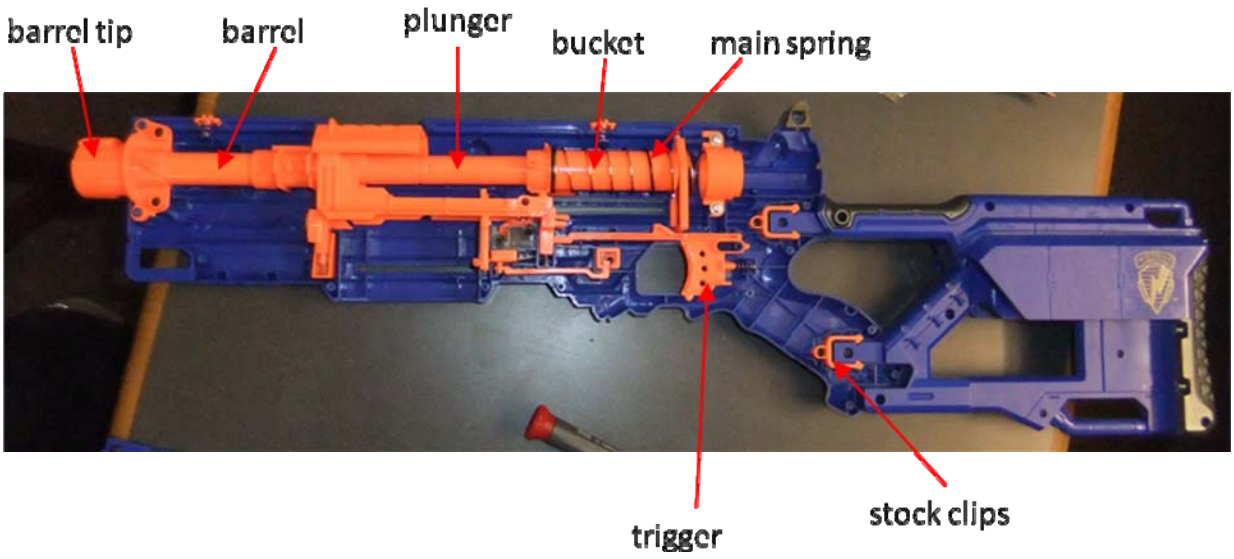

Figure 2: Internal component view

The plunger is directly connected to the bolt action rod. After the dart is loaded, the trigger releases the bucket, which is propelled forward by the compressed main spring. The released bucket creates air pressure through the plunger which propels the dart through the barrel and out the barrel tip.

The current design has weak performance in terms of power and accuracy. Testing showed that the barrel extension actually hindered the range; a 35 foot range was only achieved without the barrel extension. The barrel extension and sight were not included in the redesign.

Objectives

The objectives for the redesign of the Nerf blaster were to increase the range and accuracy and to allow for a removable stock. The improved range was specified to 70 feet. This specification was met by increasing the main spring force. The accuracy was improved by smoothing the barrel and removing the air restrictor. The stock snaps were redesigned to create two directional snapping.

Modeling – External Components

In contrast to the internal components, the external components generally involved more complexity due to the added aesthetic requirement. These external components included the left and right main body shells, the stock, the clip, and the bolt handles. The most complex by far of these components were the body shells. They share 209 common features with the left having a total of 224 features and the right having a total of 297 features. The modeling process of the external parts is discussed below.

Due to the symmetrical nature of the body shells, the left and right sides shared all of their external features and a number of internal ones. This symmetry allowed for much of the geometry to be created as a single model until differentiation was necessary. The left side of the shell was slightly simpler than the right side and was judged to be more easily morphed into the right than vice versa, this lead to the common geometry being created in the left shell orientation initially.

The external geometry was initially created as a solid model, using various layered extrudes and chamfers to create the angular look of the body. An intermediate stage of the models creation is shown in Figure 3.

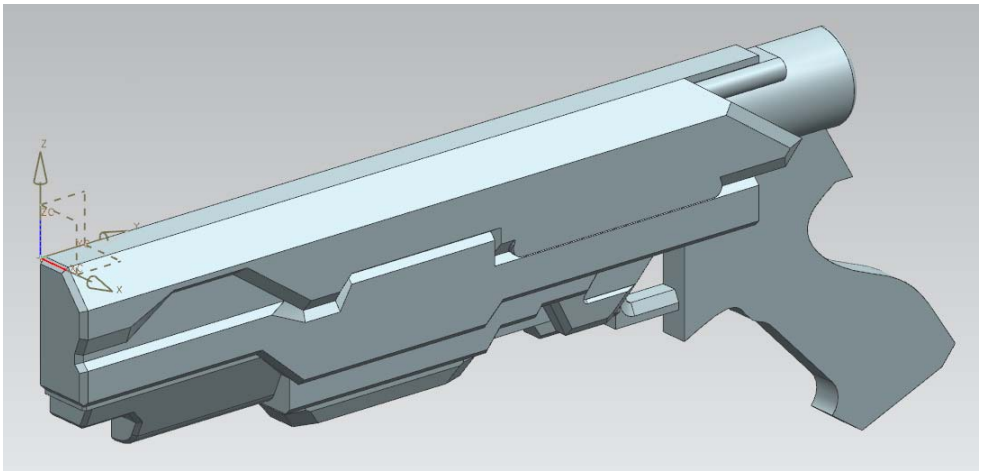

Figure 3: Shell – Intermediate stage

The handle profile was created using several 3rd order Hermite curves. Another notable feature of the exterior was the variable angle chamfer created as a sweep with three guide curves. This geometry is detailed in Figure 4.

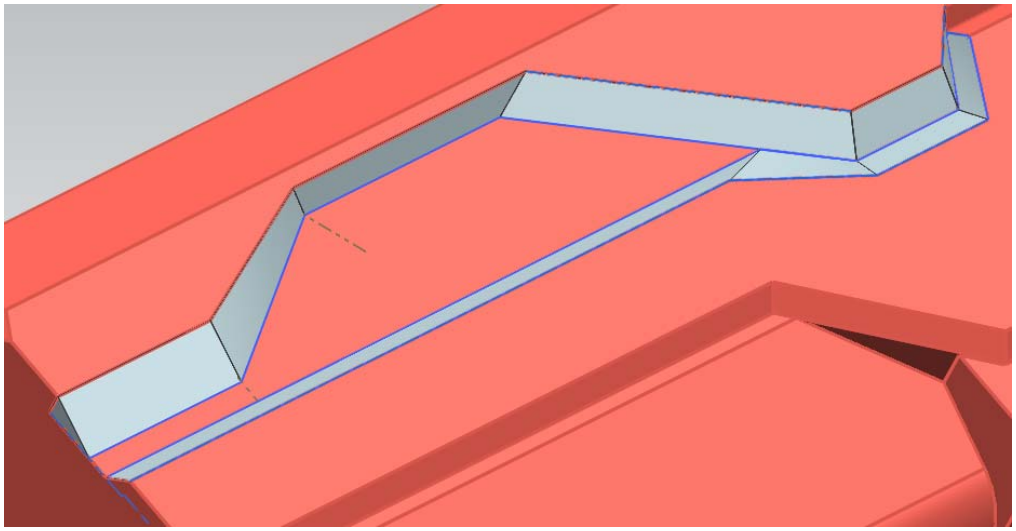

Figure 4: Sweep to create varying angle chamfer

The exterior geometry of the shell was completed by adding detail to the handle and trigger section, as shown in Figure 5.

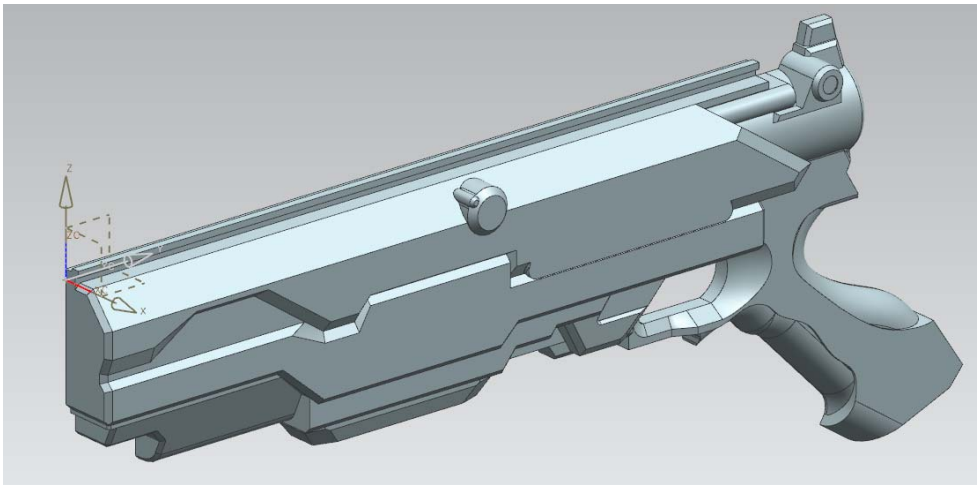

Figure 5: Completed shell exterior

The handle detail was created by first rounding the edge of the first handle extrusion, shown in Figure 3, and then extruding a second profile through the first. The second profile was also created using Hermite curves. The most complex feature in trigger-handle geometry was the cut-in at the rear of the trigger hole, shown in Figure 6. This feature was created using a sweep of the shown section along the two guide curves also shown in the figure. The sweep was then subtracted from the model to create the desired geometry.

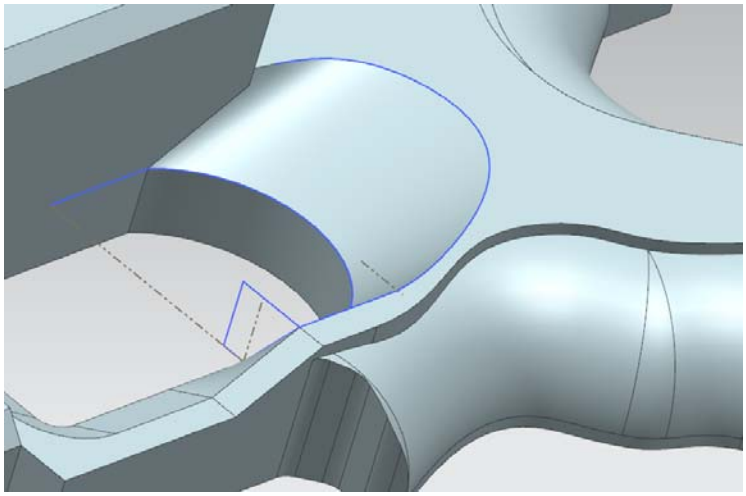

Figure 6: Trigger hole cut-in

After the external geometry was completed, the solid body was shelled to a thickness of 0.06” to allow for the internal geometry to be created. All of the internal features that were common to both the left and the right sides were then added to the model, as shown in Figure 7. First holes were added for the clip and the slider. The rest of the internal geometry was then created using the clip hole and the center line of the cylinder at the rear of the blaster as reference points. This was crucial as the majority of the internal features of the body shell served as locating features for the internal components of the blaster. The most important internal locating features were the rails for the plunger and bucket to ride in. The majority of the internal features were created as sketches on the open face of the shell that were then extruded, from various starting distances, up to the shell.

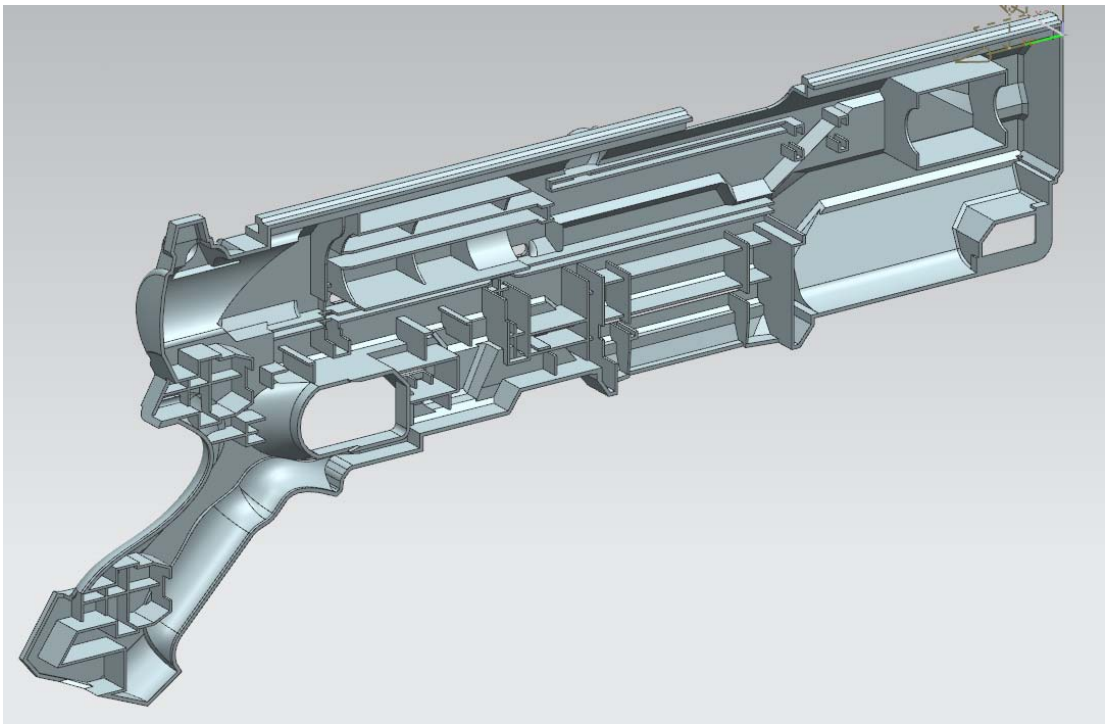

Figure 7: Common internal geometry

After all of the common features were completed, the part was differentiated into a left and right side body shell. The left side shell simply continued on from the common model, while

the right side was created by mirroring the body, uniting the two, and then trimming off the left side.

The right side body shell was slightly different internally than the left as it had the majority of the locating for the internal components. In addition to the extra geometry, much of the original geometry from the common model had to be slightly modified. The majority of these changes involved altering the height of the original features. This was accomplished using new extrudes placed on top of the originals. The internal view of the right body shell is shown in Figure 8. The cylinders that are present throughout the model serve as locating and mounting features for several internal components.

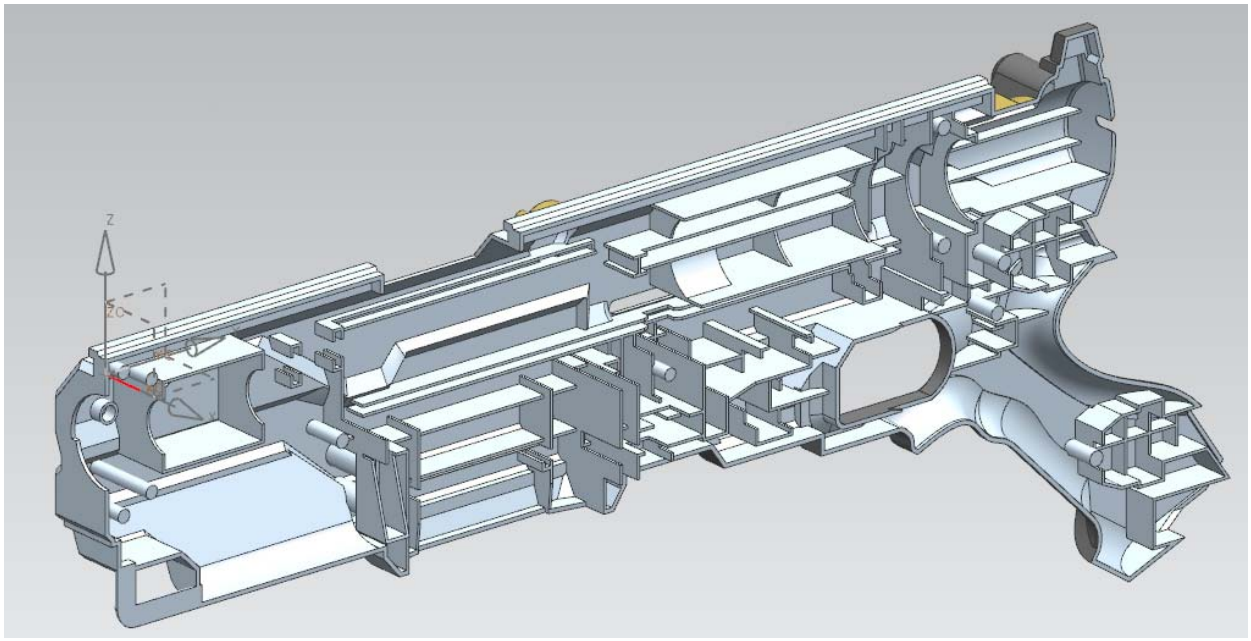

Figure 8: Finished right body shell internals

The stock was created in a similar manner as the body shells; however, the part was solid and did not require a shell. Due to the inherent symmetry of the part, the model was created as one half and then mirrored. The model was started by creating a series of overlapping extrudes of varying heights and uniting them, as shown in Figure 9. Various chamfers and round were then added to the model to refine the shape.

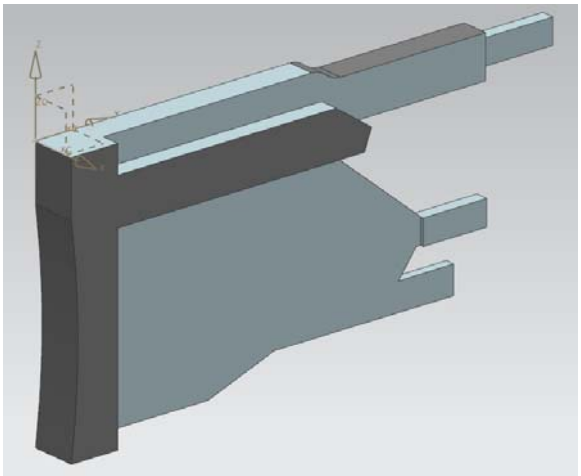

Figure 9: Stock – initial extrudes

The large overhang was created initially as an extrusion that was kept as a separate body. A chamfer was applied and the body was then shelled to a thickness of .1”. After the shell the two bodies were united. This is shown in Figure 10.

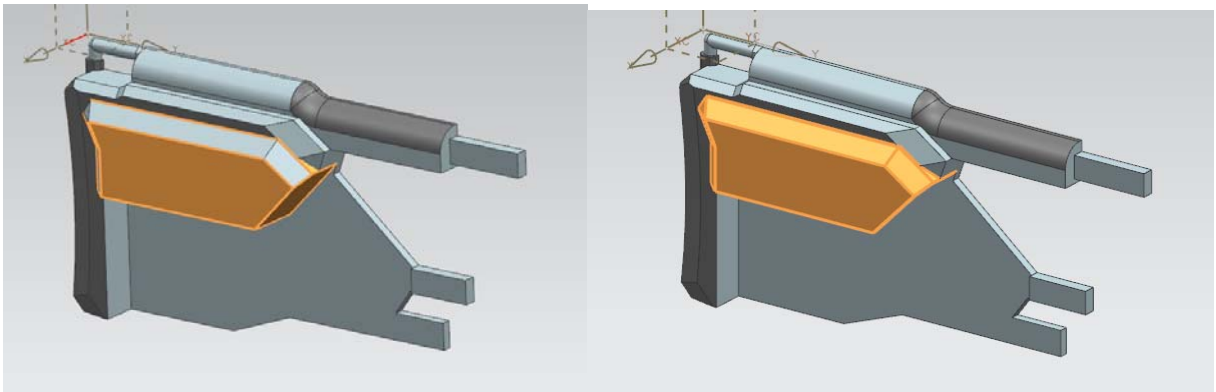

Figure 10: Stock – large overhang

The part was finalized through the addition of a few more extrudes, edge blends, and chamfers. Extrude cuts were used to alter the geometry of the part such that it would align with the main body relatively seamlessly. Finally, the part was mirrored across its central axis. The completed stock is shown in Figure 11.

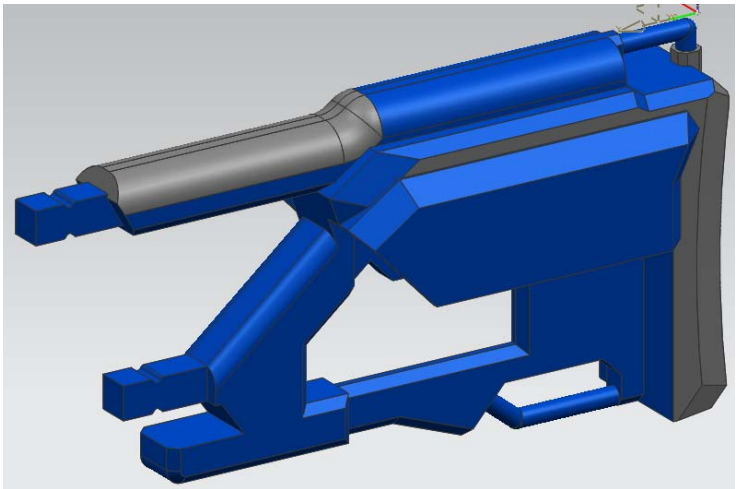

Figure 11: Stock – completed

The clip was created by first extruding one profile downward on the x-y plane and then two circular ones on the y-z plane, one normal extrude and one a cutting extrude. This is shown in Figure 12.

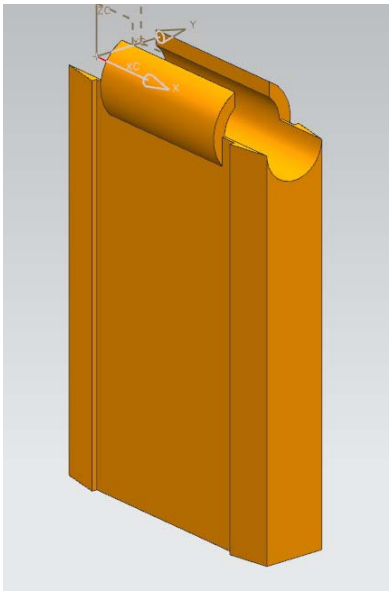

Figure 12: Clip – initial

The part was then hollowed out using a cutting extrude down through the center of the vertical body portion. External extruded features were then added and mirrored to the other side due to

the symmetry of the part. The detail at the bottom of the clip was created as a single sketch that was extrude cut into the model. The sketch is shown in Figure 13.

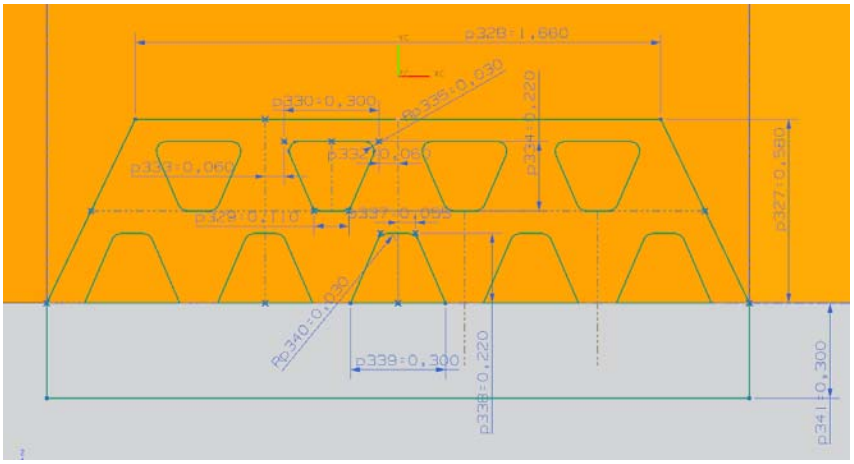

Figure 13: Clip – detail sketch

The sketch in the above figure relied was largely constructed using mirroring techniques. The top and bottom pattern were created separately. The top patterns employed two mirrors while the bottom employed three. The detail cutout feature was mirrored to the other side of the part as well. The final clip is shown in Figure 14.

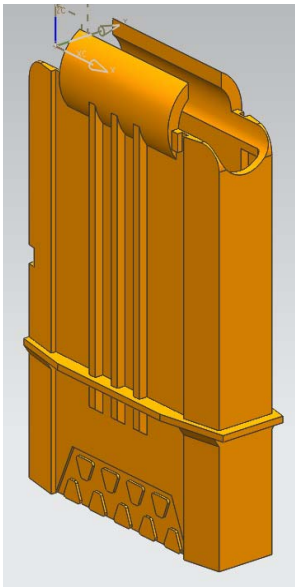

Figure 14: Clip - final

The bolt handle was started as a simple revolved section, as shown in Figure 15. The texture was then added as extrudes from the two mid-planes.

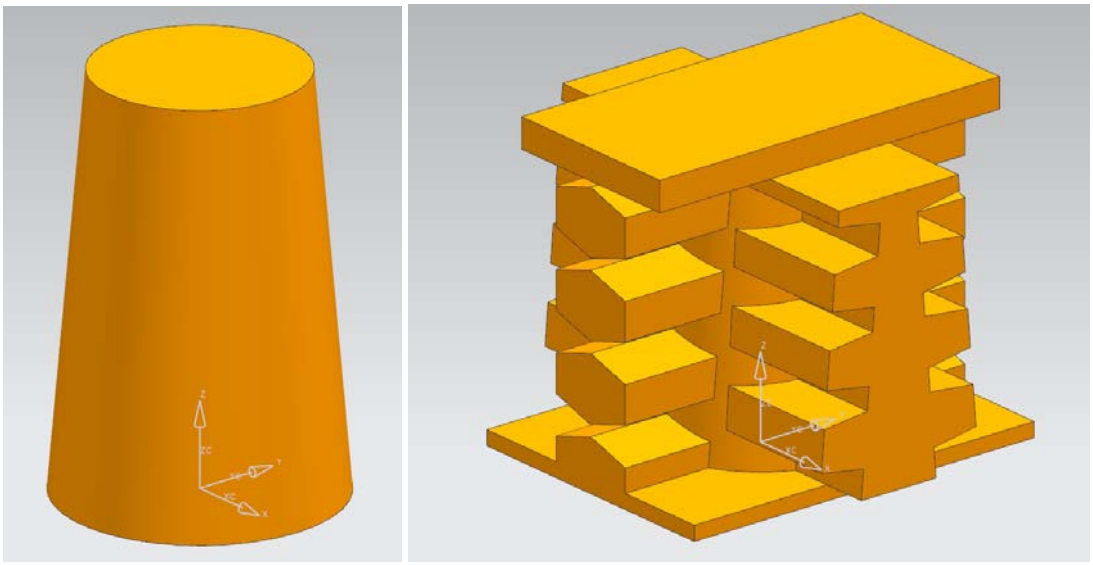

Figure 15: Bolt handle: initial and texture

The sketches for these extrudes relied heavily on mirroring and parallel constraints. The final shape of the bolt handle was then obtained by trimming the excess off the extrusions with a second revolved feature. The part was finalized through the addition of a cut extruded hole in the top and some edge blends. The final part is shown in Figure 16.

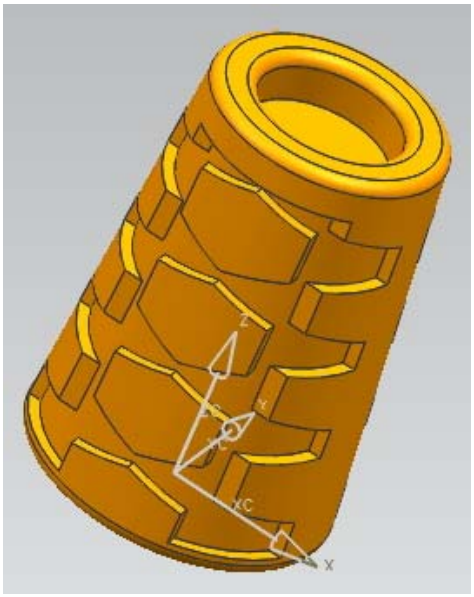

Figure 16: Bolt handle – final

The final external piece, the slider, was created initially as an extruded cross section, as shown in Figure 17. The vertical external tab was extruded and then chamfered. The holes were cut extruded using the sketch shown in Figure 18.

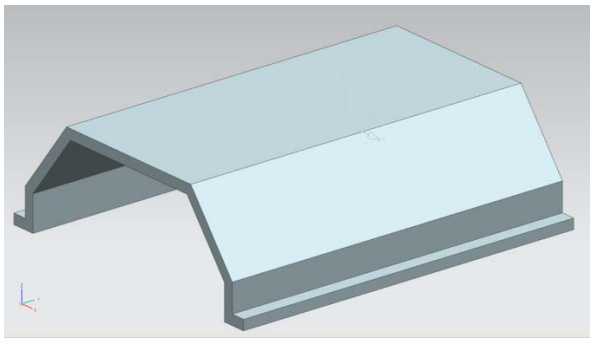

Figure 17: Slider – initial

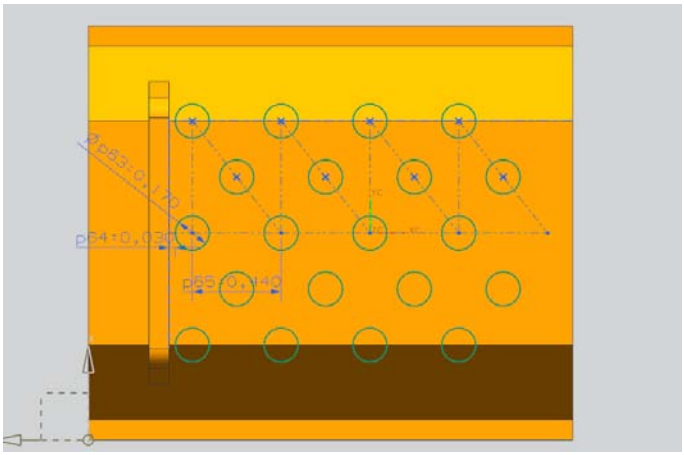

Figure 18: Slider – hole sketch

In the above figure, the hole sketch was constrained using equal length relations between the repeated triangles, equal radius relations between the circles, and by locking each circle to either an end point or midpoint. The circles are also mirrored across the mid-line. The final slider is shown in Figure 19.

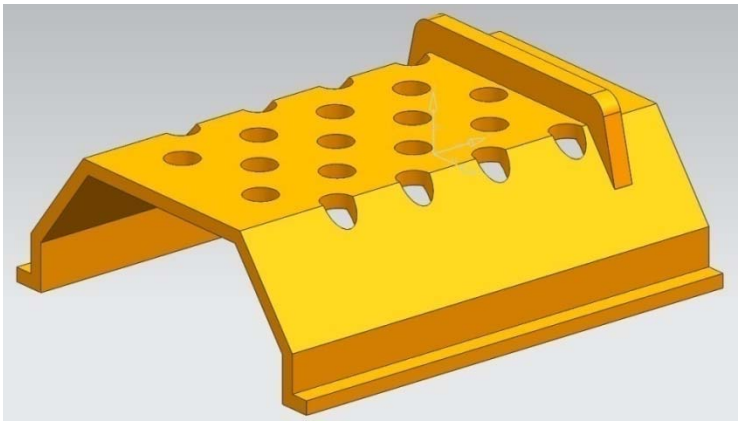

Figure 19: Slider – final

Modeling – Internal Components

The internal components were modeled using basic shapes and geometry. These parts were simple in modeling since their functionality was the only importance; they are all housed in

the main body and are not visually seen from the outside. In total, there were 32 internal components; only the modeling processes for the eight most complex parts were described.

First, the bucket was modeled as a cylinder, shown in Figure 20.

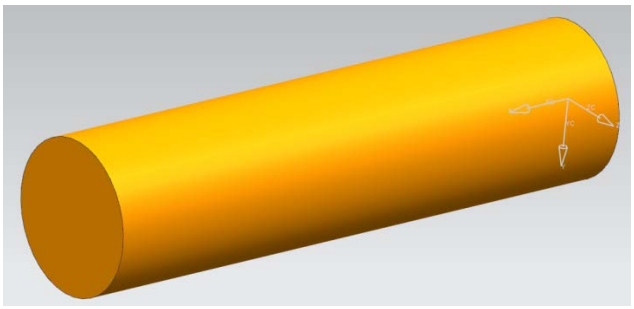

Figure 20: Bucket – cylinder

Then, the part was shelled out with a 0.050” thickness, shown in Figure 21.

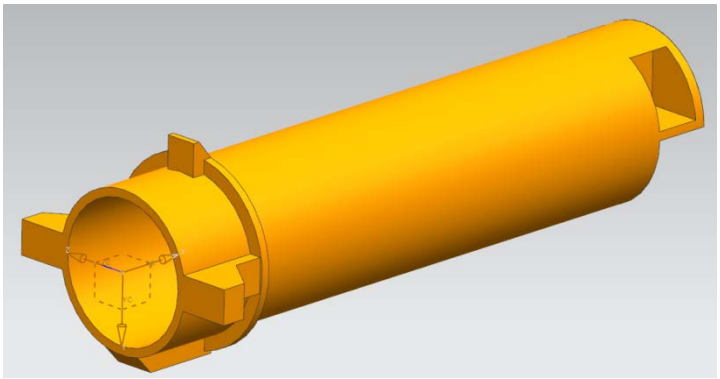

Figure 21: Bucket – final

The barrel grooves on the side were extruded and then mirrored. The restraining tab on the top was also extruded to the cylindrical outer surface.

The plunger was first modeled as a shelled box with a 0.17” thickness, shown in Figure 22.

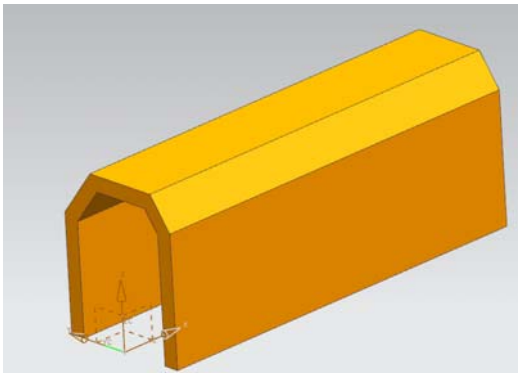

Figure 22: Plunger – shell

Then cutouts were made, and the barrel grooves were extruded, shown in Figure 23.

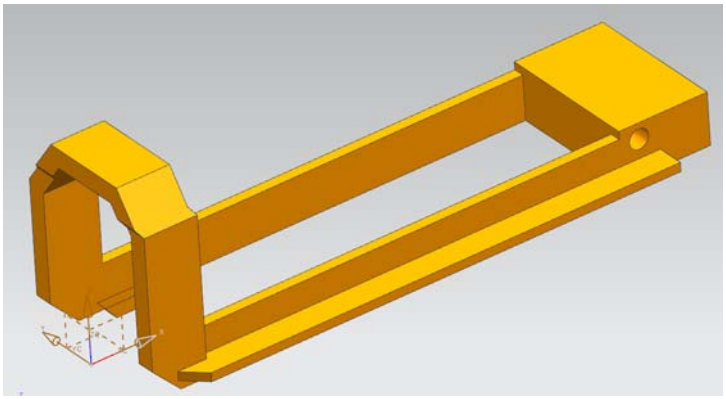

Figure 23: Plunger – cutaway

A hollow cylinder was extruded down the barrel axis, and the plunger stopper cutouts extruded, shown in Figure 24.

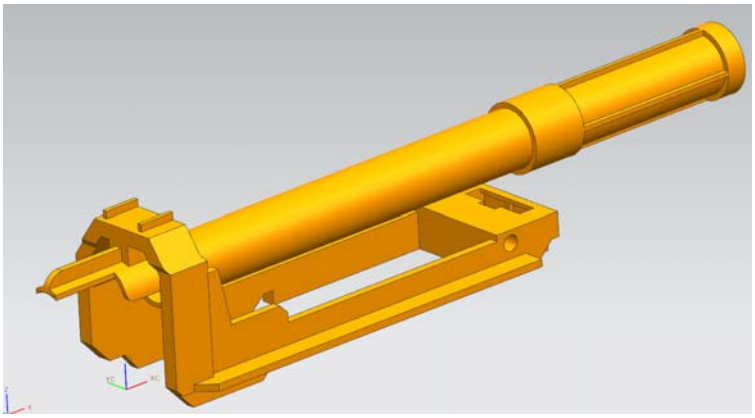

Figure 24: Plunger – final

The trigger model was started by extruding a 0.21” thick profile of the trigger arm, shown in Figure 25.

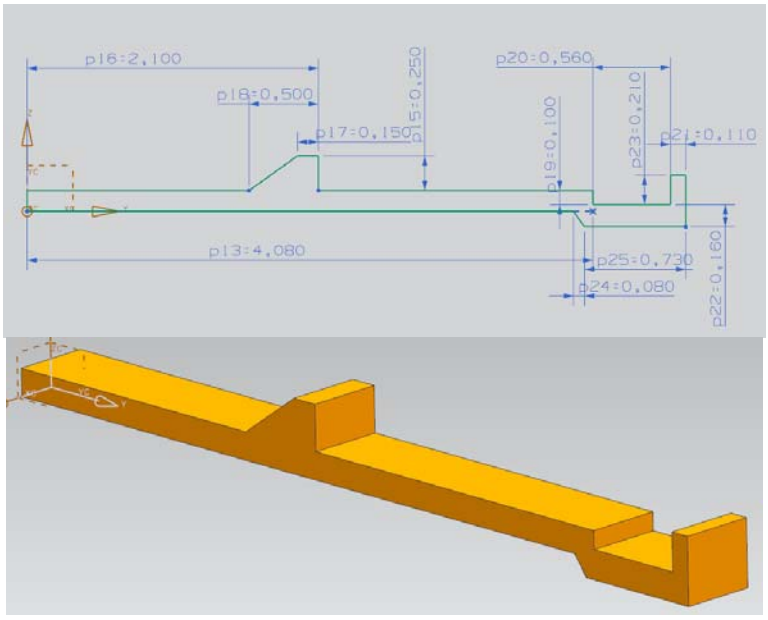

Figure 25: Trigger – arm

Then the trigger notch and handle were extruded, shown in Figure 26.

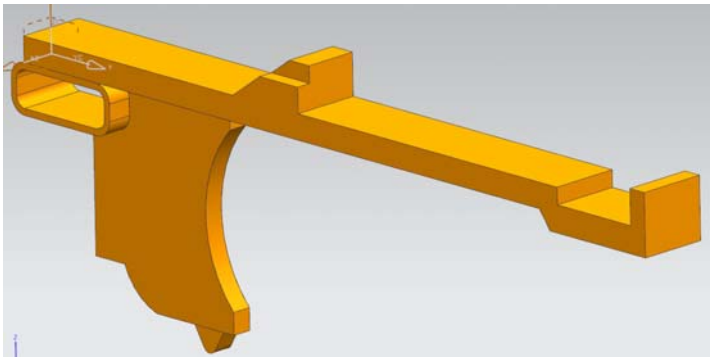

Figure 26: Trigger – notch and handle

The part was finalized by making hole cutouts, extruding platforms, and creating a grip by a swept profile, shown in Figure 27.

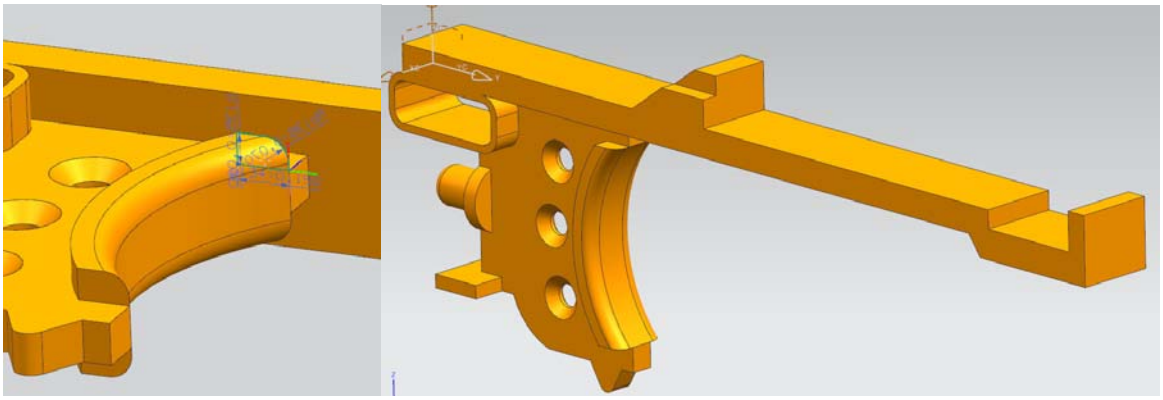

Figure 27: Trigger – final

The chamber entrance was modeled by extruding hollow cylinders, shown in Figure 28.

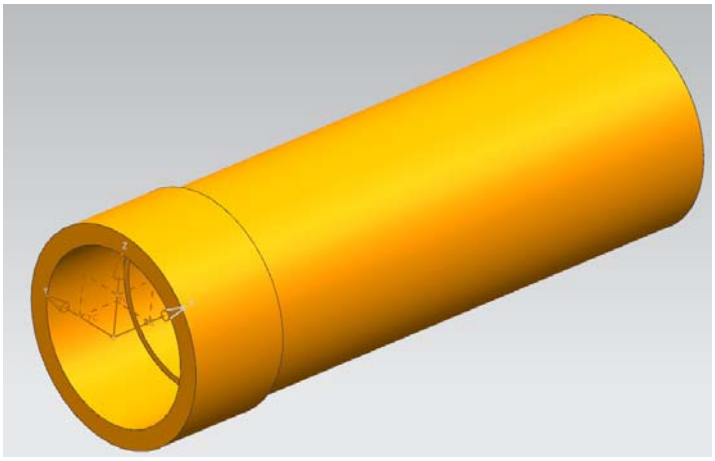

Figure 28: Chamber entrance – cylinders

Extrusions and cutouts were made at the entrance, shown in Figure 29.

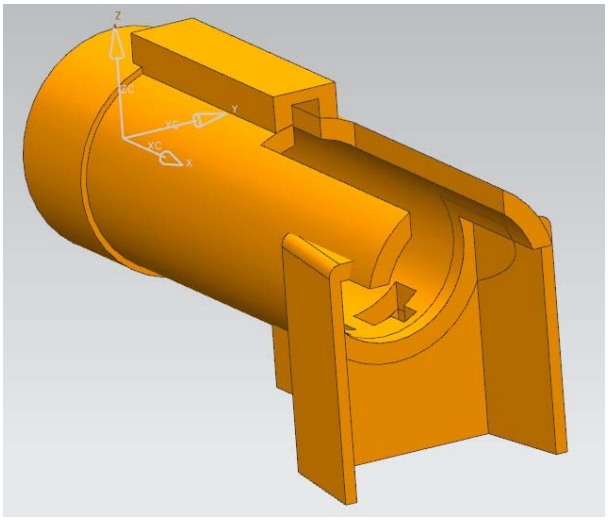

Figure 29: Chamber entrance – entrance cutouts

The barrel locating features were extruded up to the cylindrical outer surface and then mirrored twice: first in the x direction and then across the axis, shown in Figure 30.

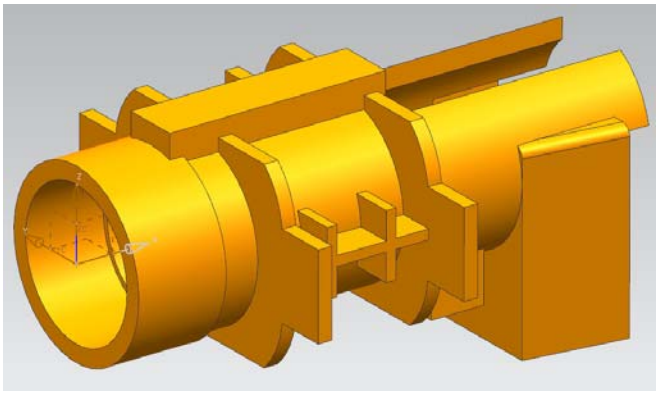

Figure 30: Chamber entrance – final

The barrel tip was first revolved about its general profile, shown in Figure 31.

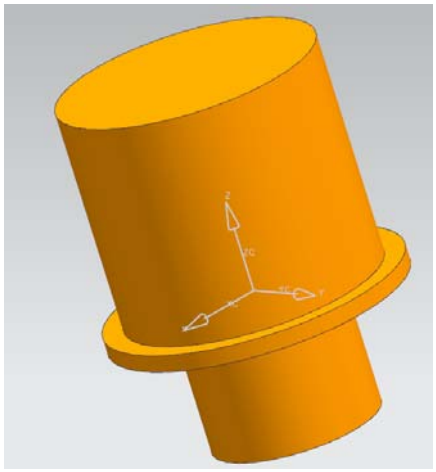

Figure 31: Barrel tip – revolve

Center and groove cutouts were made, shown in Figure 32.

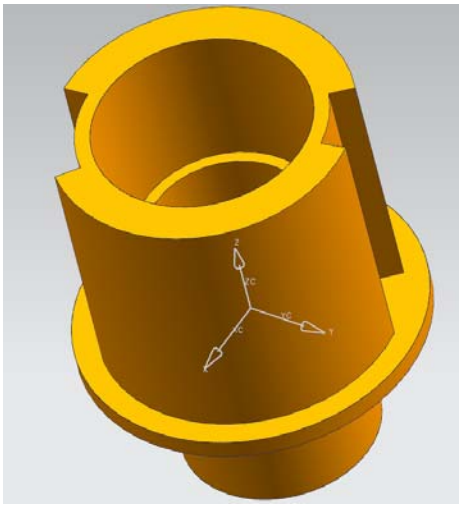

Figure 32: Barrel tip – cutouts

Locating features, including screw bosses and post holes, were extruded, shown in Figure 33.

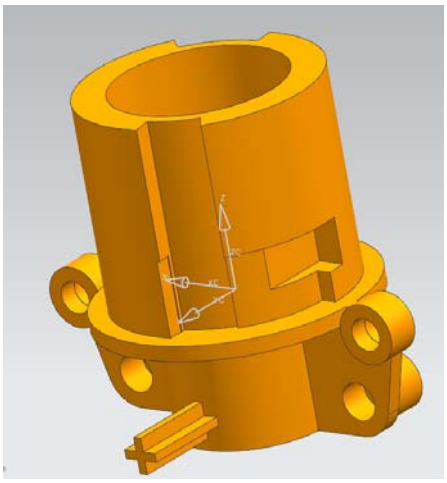

Figure 33: Barrel tip – final

The main spring stopper was also revolved about its general profile, shown in Figure 34.

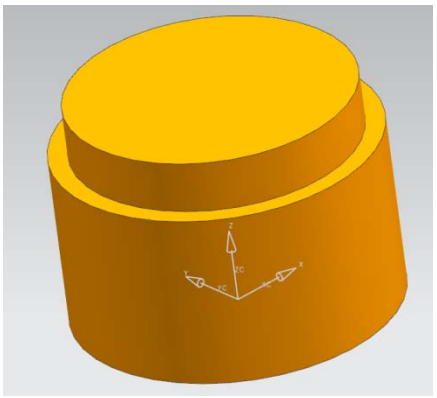

Figure 34: Main spring stopper – revolve

The part was then shelled out to a 0.075” thickness. The screw holes were extruded and then mirrored. One side had a further cut out for locating purposes, shown in Figure 35.

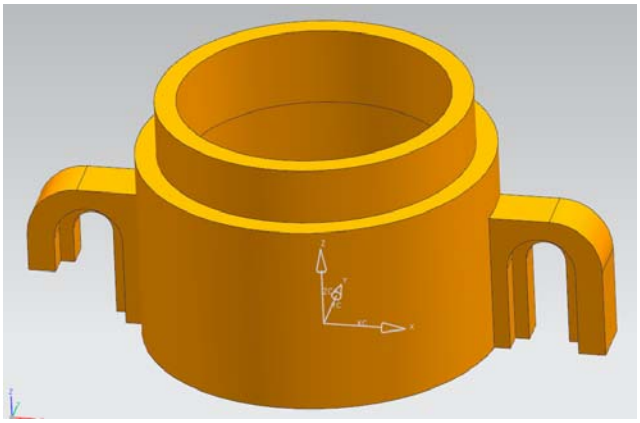

Figure 35: Main spring stopper – final

Modeling – Final Assembly

The stock snap redesign is shown in Figure 36.

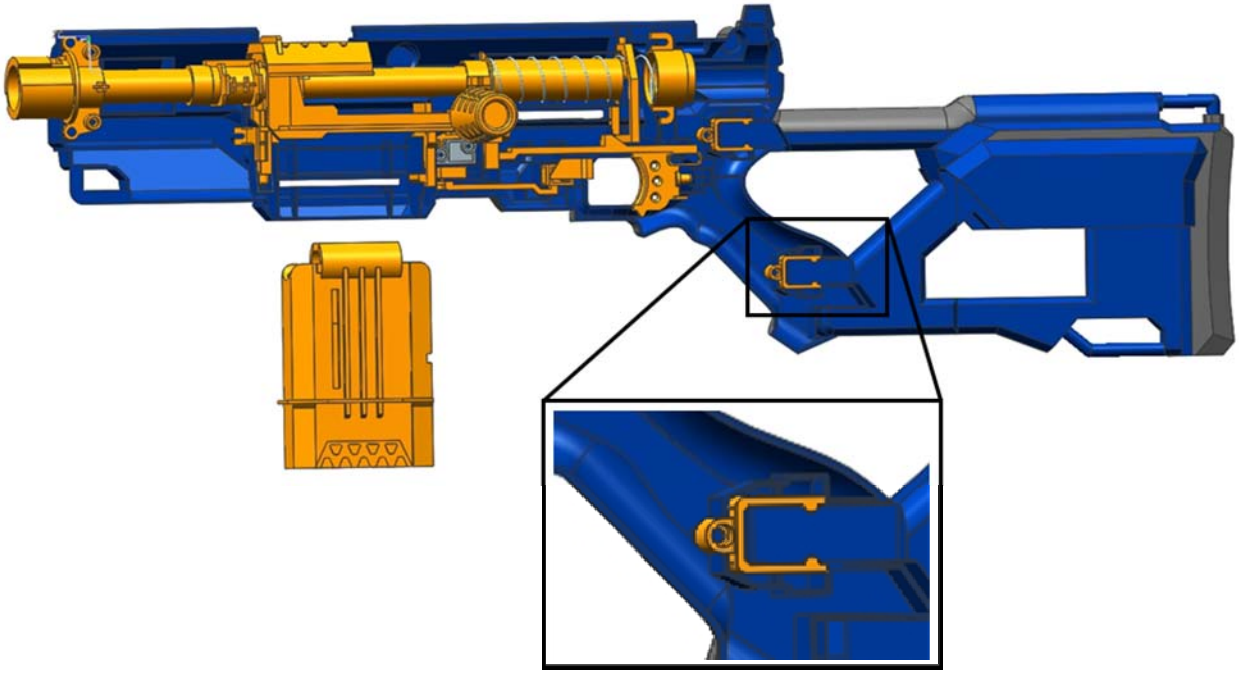

Figure 36: Stock snap redesign

The snap shape was change to a rounded snap. This snap feature allows for the stock to be removed after installation.

The final modeled assembly is shown in Figure 37.

Figure 37: Full Assembly

The assembly in general was modeled as closely to the original design as possible, retaining the same aesthetic image from the external view.

Finite Element Analysis (FEA)

FEA was conducted on two parts: the bucket and plunger. These parts receive most of the load from the increased 12 lb spring force. This force was set to be twice the original spring force of 6 lb, which was determined by measuring the spring constant. A spring constant of 1.56 lb/in was calculated by dividing a known weight by the reduction in free spring length. The main spring was measured to compress about 3.74 in. when fully loaded, so the calculated spring force was about 5.83 lb, rounded up to 6 lb. The spring force was approximated as 12 lb in all the FEA.

The Bucket

First, the bucket was divided in half down about the symmetric plane, shown in Figure 38.

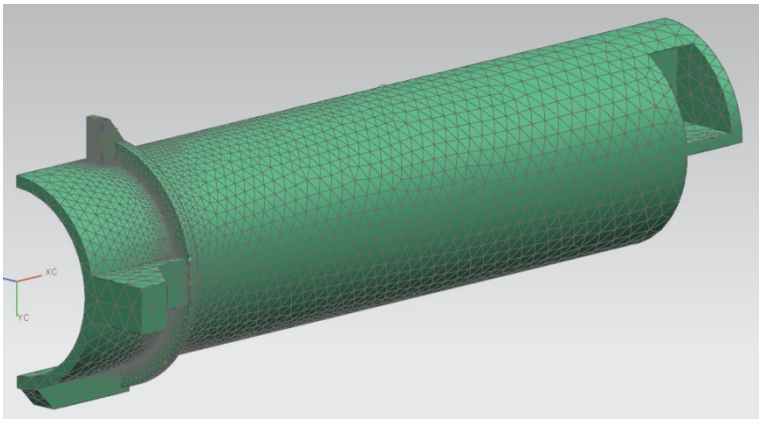

Figure 38: Bucket FEA – meshes

The entire part was first meshed with 3D tetrahedral elements 0.10” in size. The mesh was further concentrated at the weak points around the spring platform using mesh control, with about 10-50 elements on an edge, depending on the size of the edge. The material for the entire part was defined as acrylonitrile butadiene styrene (ABS) in the NX 6.0 material library.

The load and constraints were then applied. The cutting surface was constrained to be fixed in every degree of freedom except x-direction translation, due to symmetry of the cut idealized part. The inside surface at the bottom of the bucket was completely fixed. The 12 lb load was applied to the spring platform in the –x direction, shown in Figure 39.

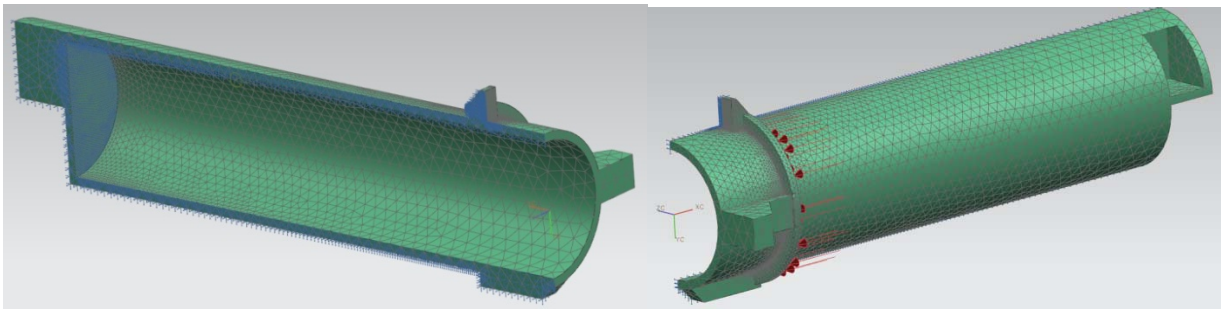

Figure 39: Bucket FEA – loads and constraints

Figure 40 shows the displacement results.

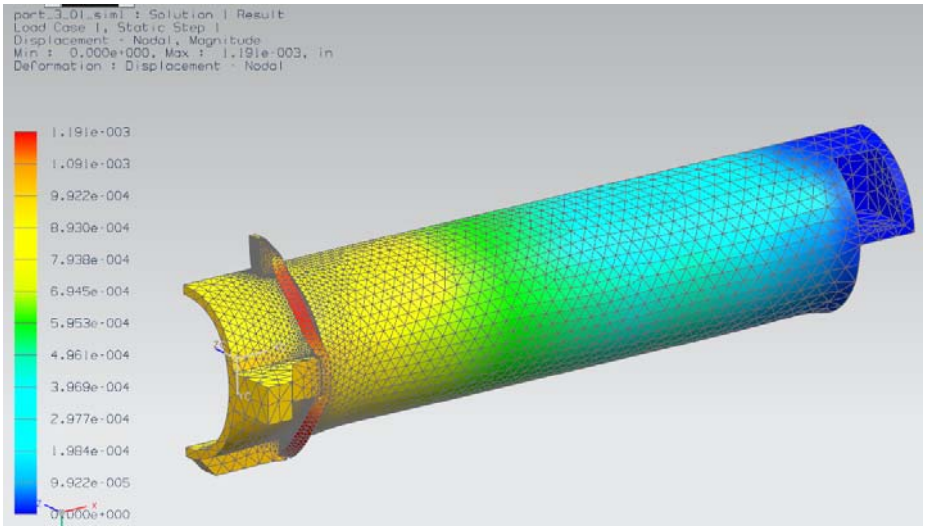

Figure 40: Bucket FEA – displacement

The largest displacement was 0.0012” and occurred at the tips of the spring platform. Figure 41 shows the Von Mises stress results.

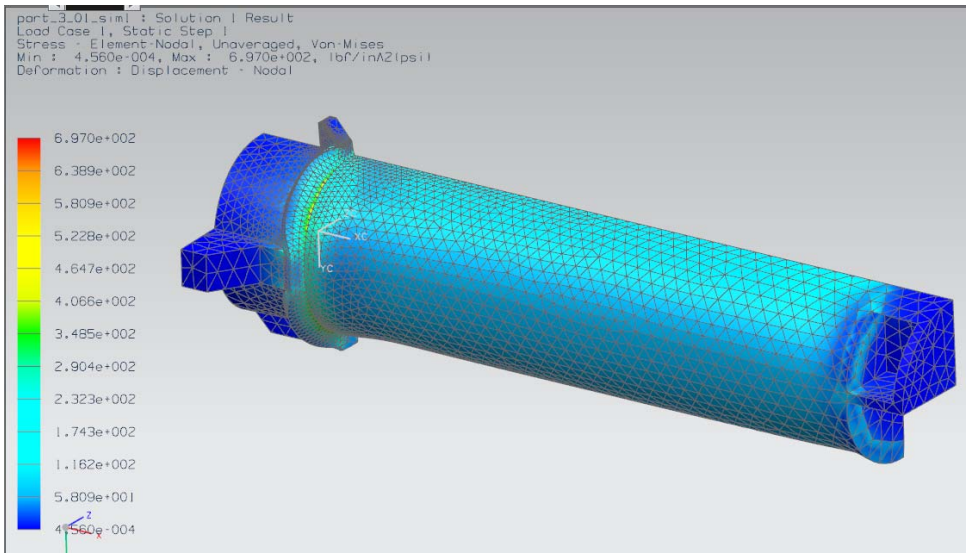

Figure 41: Bucket FEA – Von Mises Stresses

The largest stress was 697 psi and occurred at the base of the spring platform, the location of the bending stress concentration.

FEA Verification - Bucket

The bucket was examined for structural analysis in the design, and the FEA results were verified by calculating basic mechanics principles by hand. The bucket was analyzed under a loading scenario the moment just after the trigger release. Figure 42 shows a simplified cross section of the bucket.

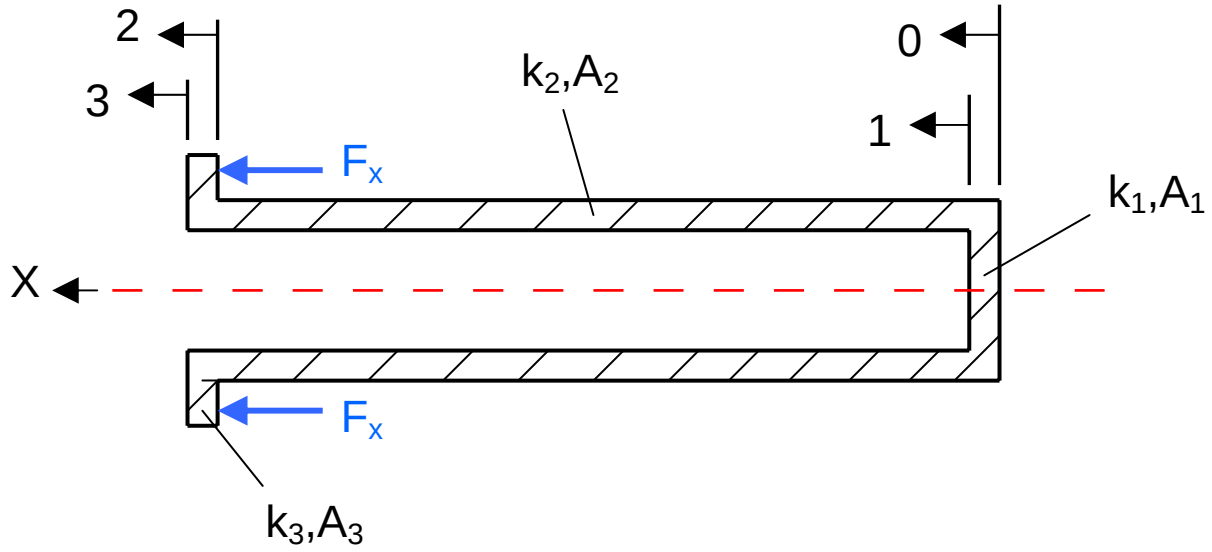

Figure 42: Bucket cross section

The part was simplified as three truss elements with varying circular cross sections. The areas A_1, A_2, and A_3 were calculated to be 0.65 in^2, 0.17 in^2, and 0.42 in^2, respectively. The spring constants k_1, k_2, and k_3 were calculated to be 4.45x10^6 lb/in, 1.94x10^4 lb/in, and 2.87x10^6 lb/in, respectively, using

$$k = \frac{AE}{L} \tag{1}$$

where k is the spring constant, A is the cross sectional area, E = 342 ksi [1] is the modulus of elasticity of ABS, and L is the length. An equivalent system of springs in series is shown in Figure 43.

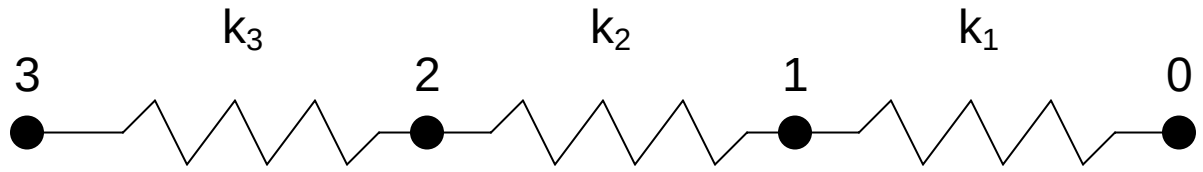

Figure 43: Spring circuit for FEA

The boundary condition was set to $d_0 = 0$. An external force F_2 = 12 lb was applied, which simulated the spring compression. The dislocations were calculated using Equation (2).

$$\begin{bmatrix} F_0 \\ F_1 \\ F_2 \\ F_3 \end{bmatrix} = \begin{bmatrix} k_1 & -k_1 & 0 & 0 \\ -k_1 & k_1+k_2 & -k_2 & 0 \\ 0 & -k_2 & k_2+k_3 & -k_3 \\ 0 & 0 & -k_3 & k_3 \end{bmatrix} \begin{bmatrix} d_0 \\ d_1 \\ d_2 \\ d_3 \end{bmatrix} \tag{2}$$

$$\begin{bmatrix} F_1 \\ F_2 \\ F_3 \end{bmatrix} = \begin{bmatrix} k_1+k_2 & -k_2 & 0 \\ -k_2 & k_2+k_3 & -k_3 \\ 0 & -k_3 & k_3 \end{bmatrix} \begin{bmatrix} d_1 \\ d_2 \\ d_3 \end{bmatrix}$$

$$\begin{bmatrix} d_1 \\ d_2 \\ d_3 \end{bmatrix} = \begin{bmatrix} k_1+k_2 & -k_2 & 0 \\ -k_2 & k_2+k_3 & -k_3 \\ 0 & -k_3 & k_3 \end{bmatrix}^{-1} \begin{bmatrix} F_1 \\ F_2 \\ F_3 \end{bmatrix}$$

$$= \begin{bmatrix} 4.45\times10^6 + 1.94\times10^4 & -1.94\times10^4 & 0 \\ -1.94\times10^4 & 1.94\times10^4 + 2.87\times10^6 & -2.87\times10^6 \\ 0 & -2.87\times10^6 & 2.87\times10^6 \end{bmatrix}^{-1} \frac{lb}{in} \begin{bmatrix} 0 \\ 0 \\ 12 \end{bmatrix} lb = \begin{bmatrix} 2.70\times10^{-6} \\ 6.21\times10^{-4} \\ 6.21\times10^{-4} \end{bmatrix} in$$

The greatest dislocation occurred at $d_2 = d_3 = 0.000625$ in. The largest FEA displacement was 0.0012" (Figure 40). This displacement was larger than the calculated displacement and was due to the additional bending deflection not accounted for in the simplified truss elements. A more accurate comparison is made at the base of the spring platform (location 2), where the FEA displacement was about 0.0009 in., on the same order of magnitude as the calculations. Both the FEA and calculated displacements were very small.

Another important verification was the stress analysis. Figure 41 showed the largest stress to be 697 psi. This stress point was caused by the bending moment of the spring platform. The yield strength of ABS was referenced to be 6266 psi [1]. The highest stress in the part was much lower than the yield strength, so the part will not fail or permanently deform under the initial loading conditions. The part will also not fail under cyclic loading conditions since the highest stress was also much lower than half of the yield strength, 3133 psi.

The Plunger

To begin the analysis, the plunger was first meshed using 3D tetrahedral elements 0.04" in size. The resulting mesh is shown in Figure 44. As with the bucket, the material was defined as ABS using the NX 6.0 material library.

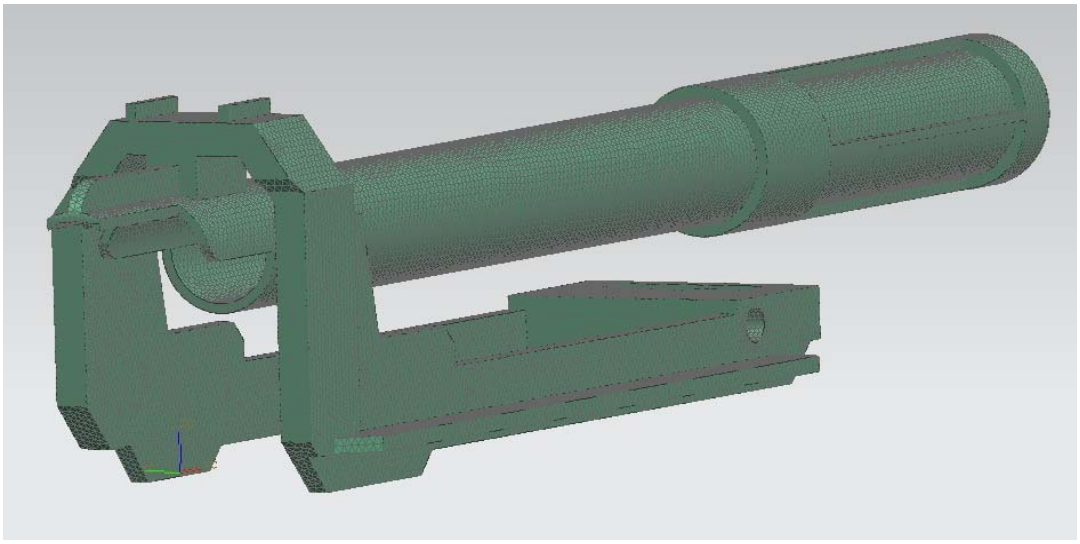

Figure 44: Plunger FEA – meshes

The plunger is the internal part of the Nerf blaster responsible for the compression of the spring. It is attached to external handles, via the through hole in the lower right hand corner Figure 44, that the user uses to pull back the spring. As the user pulls back on the handles the far end of the tube pushes on the bucket which compresses the spring. Due to this, the part must support the spring force generated by full compression. To replicate this loading condition, loads and constraints were then applied to the mesh. The far end of the tube was fixed and a bearing load equivalent to the fully compressed spring force, 12 lbs, was applied to through hole. Additionally, the upper faces of the two fins that run the length of the lower “L” shape were constrained to only allow motion in the x-direction. This was to replicate the rails in which the fins run. The loads and constraints are shown in Figure 45.

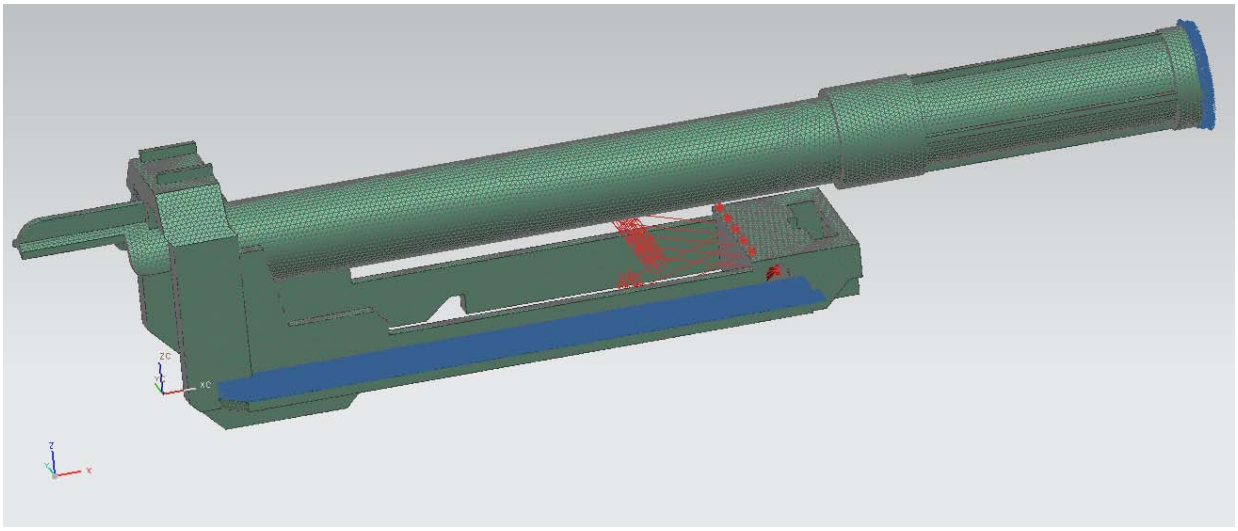

Figure 45: Plunger FEA – loads and constraints

The FEA analysis was then performed. The displacement magnitude results are shown in Figure 46.

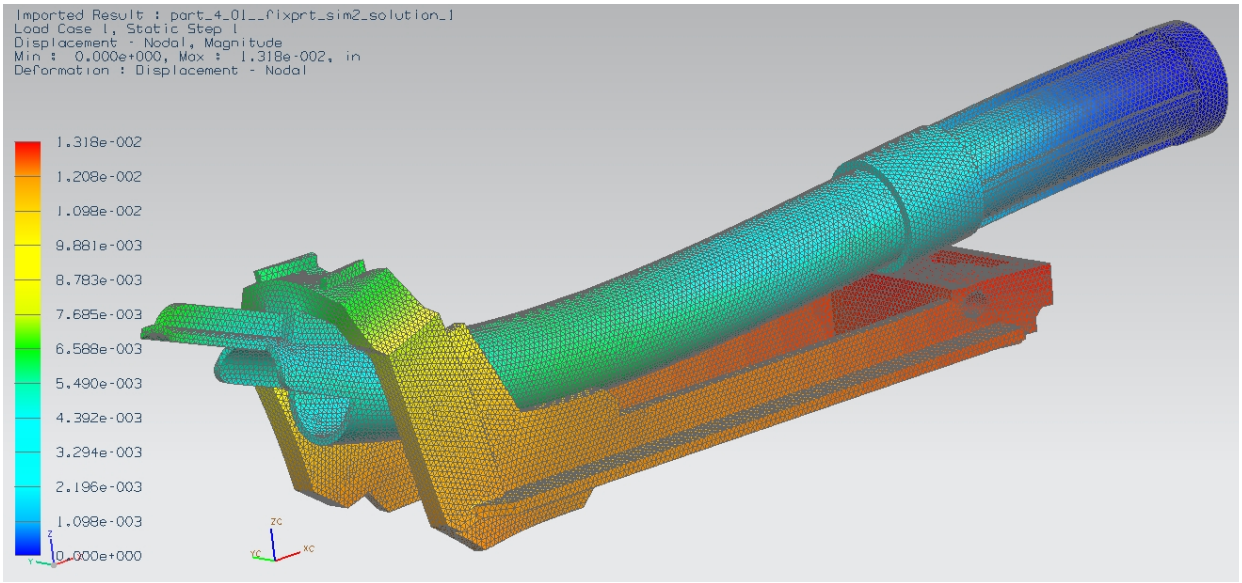

Figure 46: Plunger FEA – displacement magnitude

The maximum displacement was .01318 in. and was located at the end of the lower “L” arms. To better examine the directionality the displacement in the x-direction and in the z-direction are shown in Figure 47 and 48 respectively.

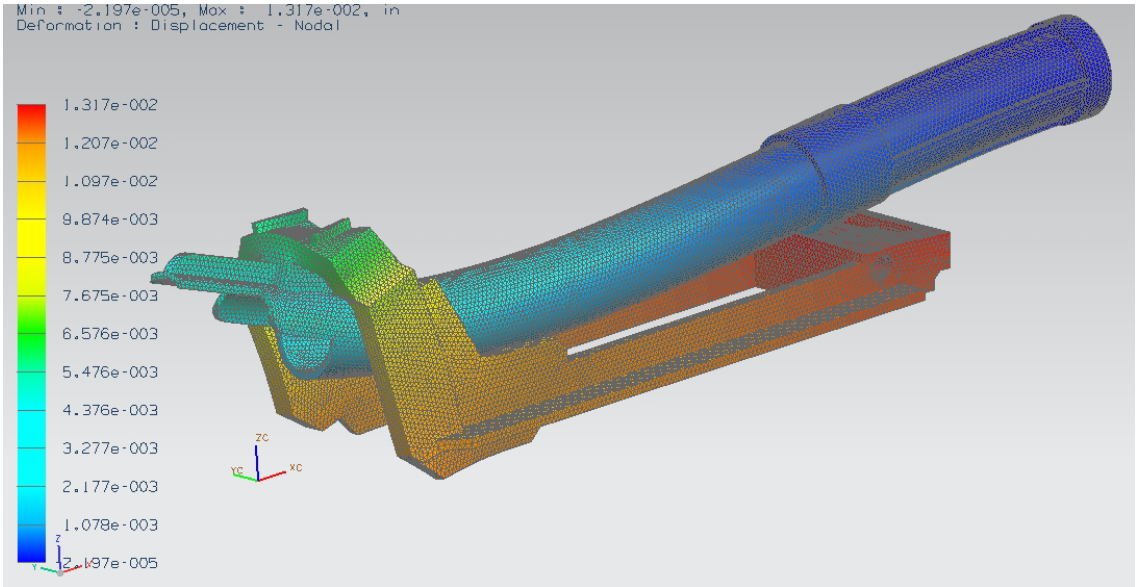

Figure 47: Plunger FEA – displacement x-direction

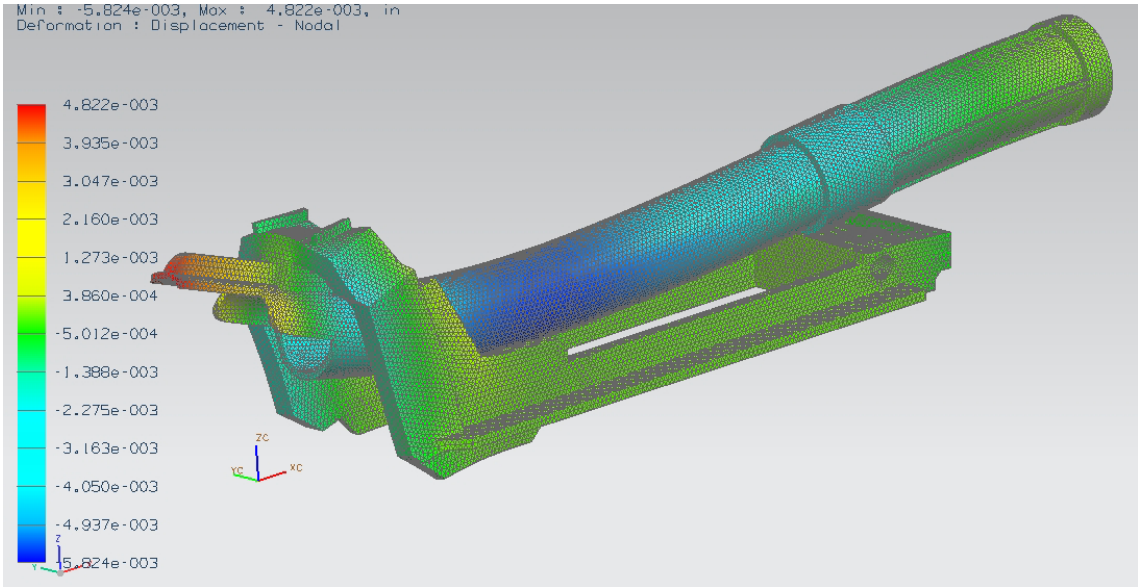

Figure 48: Plunger FEA – displacement z-direction

The maximum displacement in the x-direction was .01317 in. again occurring at the end on the lower “L” arms. The maximum displacement in the y direction was -.005824 in., occurring towards the center of the tube. The Von Mises stress results are shown in Figure 49.

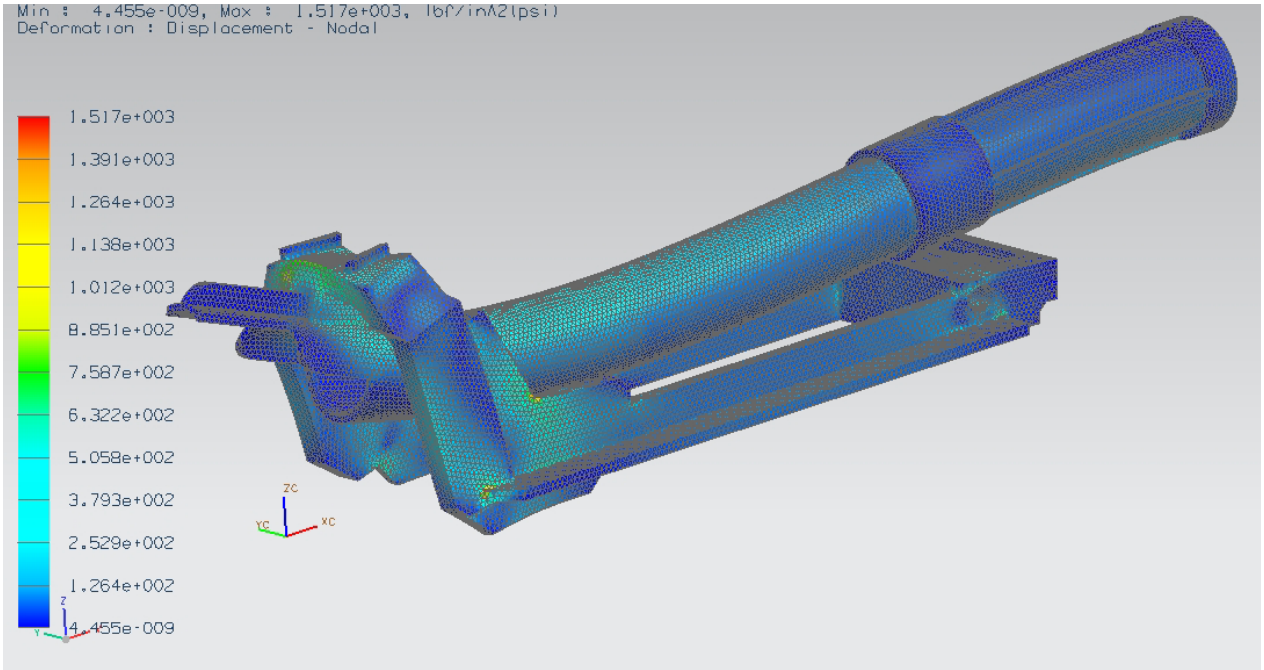

Figure 49: Plunger FEA – Von Mises Stresses

The largest stress was 1517 psi and occurred at the corner of the vertical “L” arms and the end of the lateral fins.

FEA Verification - Plunger

The plunger was examined for structural analysis in the design, and the FEA results were verified by calculating basic mechanics principles by hand. The plunger geometry was simplified to facilitate the hand calculations. As part of this simplification the part was broken into four separate parts. Each sub-part was assumed to be fixed at the interface between it and the next

part. In this manner the displacements of each part were calculated relative to the sub-part before it. After the calculations were completed the sub-part displacements were combined to find the true displacements.

The first part was the lower arm of the "L" bracket. A cross section of this simplified geometry is shown in Figure 50.

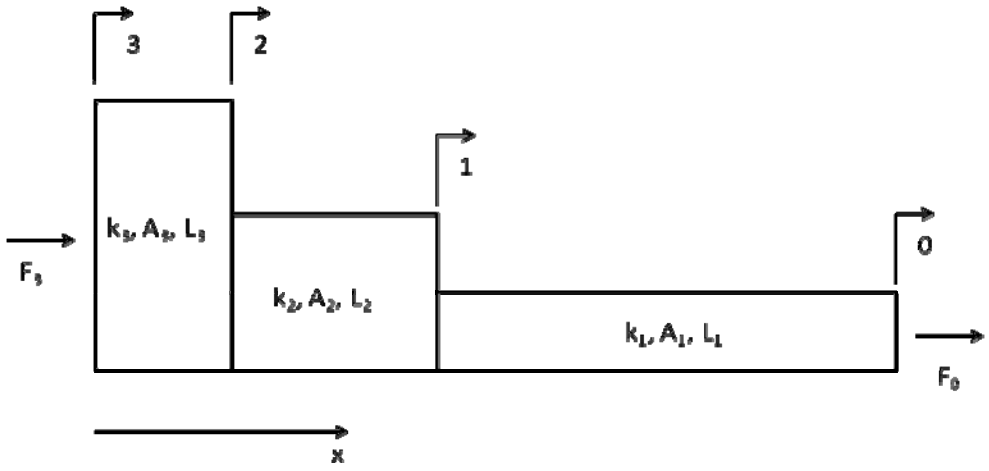

Figure 50: Plunger simplified geometry part 1

The areas A_1, A_2, and A_3 were calculated to be 0.12 in^2, 0.186 in^2, .316 in^2, incorporating the widths of both "L" brackets. The lengths L_1, L_2, and L_3 were found to be 3.03 in, 0.76 in, 0.59 in respectively. The spring constants k_1, k_2 and k_3 were calculated to be 13544.55 lb/in, 83700 lb/in, 183172.9 lb/in using Equation 1 and the modulus of elasticity specified earlier. An equivalent system of springs in series for this part is shown in Figure 51.

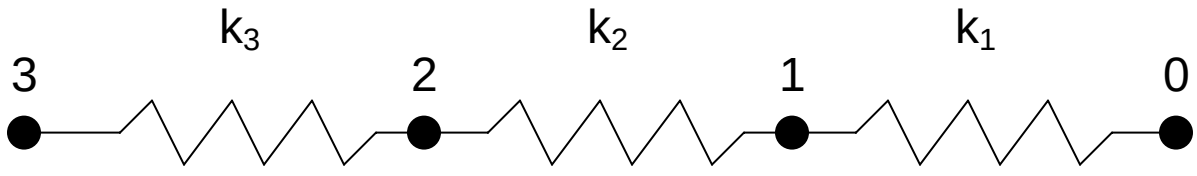

Figure 51: Sub-part 1 Spring Circuit for FEA

This sub-part was assumed to be fixed at node 3 for calculations. The boundary conditions were set to $d_3 = 0$ and an external force $F_0 = 12$ lbs was applied, representing the pulling force. The dislocations relative to node 3 were found using

$$\begin{bmatrix} F_0 \\ F_1 \\ F_2 \\ F_3 \end{bmatrix} = \begin{bmatrix} k_1 & -k_1 & 0 & 0 \\ -k_1 & k_1+k_2 & -k_2 & 0 \\ 0 & -k_2 & k_2+k_3 & -k_3 \\ 0 & 0 & -k_3 & k_3 \end{bmatrix} \begin{bmatrix} d_0 \\ d_1 \\ d_2 \\ d_3 \end{bmatrix} \tag{3}$$

$$\begin{bmatrix} F_0 \\ F_1 \\ F_2 \end{bmatrix} = \begin{bmatrix} k_1 & -k_1 & 0 \\ -k_1 & k_1+k_2 & -k_2 \\ 0 & -k_2 & k_2+k_3 \end{bmatrix} \begin{bmatrix} d_0 \\ d_1 \\ d_2 \end{bmatrix}$$

$$\begin{bmatrix} d_0 \\ d_1 \\ d_2 \end{bmatrix} = \begin{bmatrix} k_1 & -k_1 & 0 \\ -k_1 & k_1+k_2 & -k_2 \\ 0 & -k_2 & k_2+k_3 \end{bmatrix}^{-1} \begin{bmatrix} F_0 \\ 0 \\ 0 \end{bmatrix}$$

d_0, d_1, and d_2 relative to node 3 were found to be 0.001 in, .0002 in, and 6.55E-05 in respectively. The force F_3 was found to be -12 lbs using

$$F_3 = -k_3 \cdot d_3 \tag{4}$$

The second sub-part was the vertical arm of the “L” bracket. It was assumed to be a vertical rectangular beam. The base, *b*, of the beam’s cross section included the thickness of both sides of the bracket and was found to be 0.34 in. The height of the beam’s cross section was found to be 0.5 in. The length of the beam, L, was assumed to be 1.45 in. These values were used to calculate the second moment of area, *I*, for the beam as

$$I = \frac{b \cdot h^3}{12} \tag{5}$$

I was found to be 0.00354 in^4 for the beam. The beam’s nodes, orientation, and loading condition are shown in Figure 52. The beam was considered fixed at node 4 on the top. The boundary

conditions were set to $d_4 = 0$ and a load $F_3 = 12$ lbs, transferred from sub-part 1, was applied. Additionally, a moment $M_4 = -8.28\ \text{lb} \cdot \text{in}$ transferred from sub-part 3 was applied at node 4.

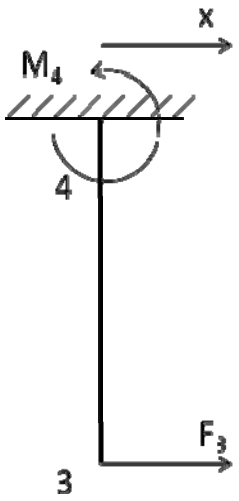

Figure 52: Sub-part 2 beam element for FEA

The displacement of node 3 relative to node 4 was then calculated using Equation 6 where the modulus of elasticity, E, is as specified earlier and the displacement angles of each node are θ_3 and θ_4.

$$\begin{bmatrix} F_4 \\ M_4 \\ F_3 \\ M_3 \end{bmatrix} = \frac{EI}{L^3}\begin{bmatrix} 12 & 6L & -12 & 6L \\ 6L & 4L^2 & -6L & 2L^2 \\ -12 & -6L & 12 & -6L \\ 6L & 2L^2 & -6L & 4L^2 \end{bmatrix}\begin{bmatrix} d_4 \\ \theta_4 \\ d_3 \\ \theta_3 \end{bmatrix} \tag{6}$$

$$\begin{bmatrix} M_4 \\ F_3 \\ M_3 \end{bmatrix} = \frac{EI}{L^2}\begin{bmatrix} 4L^2 & -6L & 2L^2 \\ -6L & 12 & -6L \\ 2L^2 & -6L & 4L^2 \end{bmatrix}\begin{bmatrix} \theta_4 \\ d_3 \\ \theta_3 \end{bmatrix}$$

$$\begin{bmatrix} \theta_4 \\ d_3 \\ \theta_3 \end{bmatrix} = \frac{EI}{L^3}\begin{bmatrix} 4L^2 & -6L & 2L^2 \\ -6L & 12 & -6L \\ 2L^2 & -6L & 4L^2 \end{bmatrix}^{-1}\begin{bmatrix} M_4 \\ F_3 \\ 0 \end{bmatrix}$$

θ_4, d_3, and θ_3 were found to be 0.0066, 0.0117 in, and 0.0061 respectively. The force at node 4 was found to be -12 lbs using

$$F_4 = \frac{EI}{L^3}[6L \quad -12 \quad 6L]\begin{bmatrix}\theta_4\\ d_5\\ \theta_5\end{bmatrix} \tag{7}$$

The third sub-part was the vertical connection between the horizontal cylinder and the top of the "L" bracket. This sub-part was also modeled as a vertical rectangular beam element. The base, height, and length were .28 in, .5 in, and .69 in respectively. The second moment of inertia was again calculated using Equation 5 and was found to be 0.00292 in^4. The beam's nodes, orientation, and loading condition are shown in Figure 53. The beam was considered fixed at node 5 on the bottom. The boundary conditions were set to $d_5 = 0$ and a load $F_4 = 12\ lbs$, transferred from sub-part 2, was applied. Additionally, a moment $M_4 = 17.4\ lb \cdot in$ transferred from sub-part 2 was applied at node 4.

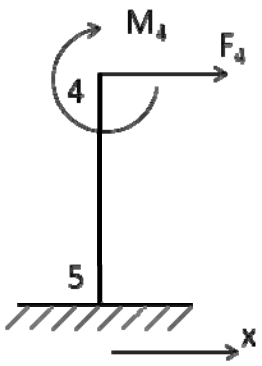

Figure 53: Sub-part 3 beam element for FEA

The displacement of node 4 relative to node 5 was then calculated using Equation 8 where the modulus of elasticity, E, is again as specified earlier and the displacement angles of each node are θ_4 and θ_5.

$$\begin{bmatrix}F_4\\ M_4\\ F_5\\ M_5\end{bmatrix} = \frac{EI}{L^3}\begin{bmatrix}12 & 6L & -12 & 6L\\ 6L & 4L^2 & -6L & 2L^2\\ -12 & -6L & 12 & -6L\\ 6L & 2L^2 & -6L & 4L^2\end{bmatrix}\begin{bmatrix}d_4\\ \theta_4\\ d_5\\ \theta_5\end{bmatrix} \tag{8}$$

$$\begin{bmatrix} F_4 \\ M_4 \\ M_5 \end{bmatrix} = \frac{EI}{L^3}\begin{bmatrix} 12 & 6L & 6L \\ 6L & 4L^2 & 2L^2 \\ 6L & 2L^2 & 4L^2 \end{bmatrix}\begin{bmatrix} d_4 \\ \theta_4 \\ \theta_5 \end{bmatrix}$$

$$\begin{bmatrix} d_4 \\ \theta_4 \\ \theta_5 \end{bmatrix} = \frac{EI}{L^3}\begin{bmatrix} 12 & 6L & 6L \\ 6L & 4L^2 & 2L^2 \\ 6L & 2L^2 & 4L^2 \end{bmatrix}\begin{bmatrix} F_4 \\ M_4 \\ M_5 \end{bmatrix}$$

d_5, θ_4, and θ_5 were found to be 0.0007 in, 0.0041, and -0.0051 respectively. The force at node 5 was found to be -12 lbs using

$$F_4 = \frac{EI}{L^3}\begin{bmatrix} -12 & -6L & -6L \end{bmatrix}\begin{bmatrix} d_4 \\ \theta_4 \\ \theta_5 \end{bmatrix} \quad (9)$$

The fourth sub-part was the horizontal tube which was modeled as a single spring element. The area and length used were .0942 in^2 and 7.29 in respectively. The spring constant, k_6, was calculated to be 4421.501 lb/in using Equation 1. The spring element and its loading condition are shown in Figure 54. The beam was considered fixed at node 6. The boundary conditions were $d_6 = 0$ and $F_5 = 12$ lbs .

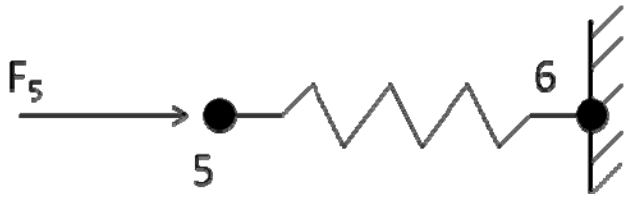

Figure 54: Sub-part 4 spring element for FEA

The displacement for node 5 was then calculated using Equation 10 and was found to be 0.002714 in.

$$d_5 = \frac{F_5}{k_6} \quad (10)$$

The force at node 6 was assumed to be equal and opposite the force at node 5, and thus was found to be -12 lbs.

The complete node structure of the plunger is shown in Figure 55. Moving in a counter clockwise direction from node 6 to node 0, the relative displacements of each node were combined to find the true displacement values. The true displacement values are shown in Table 1.

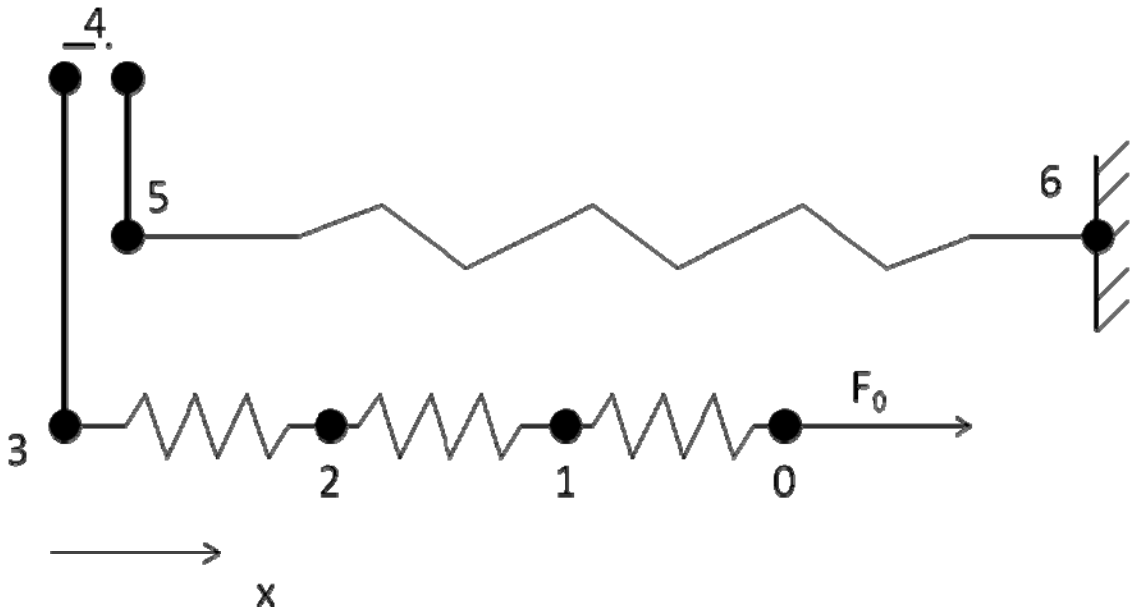

Figure 55: Plunger Node Structure for FEA

Table 1: True Plunger Displacement Values

Node	Displacement (in)
0	0.01621
1	0.01532
2	0.01518
3	0.01511
4	0.00341
5	0.00271
6	0.00000

The calculated displacement at node 0 was found to be 0.01621 in. This is comparable to the NX 6.0 calculated result of .01318 in for the same location. The similarity between the two numbers lends validity to the results obtained using the NX software.

Conclusions

The redesign of the Nerf Longstrike CS-6 was based on an increased spring force of 12 lb. Two components, the bucket and plunger, were analyzed for structural integrity with this increased loading. FEA was conducted, and the maximum displacements for the bucket and plunger were 0.0012” and 0.013”, respectively. The maximum internal stresses (Von Mises) were 697 psi and 1517 psi for the bucket and plunger, respectively. These values were much lower than both the yield strength of ABS (6266 psi) and half the yield strength (3133 psi),

which suggests the parts' abilities to withstand fatigue loading. The FEA results were also verified using basic mechanics principles.

Some changes were made to internal components. The stock snaps were redesigned to be rounded snaps to allow for stock removal. In addition, the inside barrel surface was smoothed out and the air restrictor in the plunger was removed in order to increase the accuracy and range of the blaster.

Future work on this redesign is necessary in order to make the design fully functional. Primarily, the screws, screw bosses, and internal springs (other than the main spring) will need to be included in the assembly. These critical components were not a part of this project due to the limited time scope. Another design step would be to prototype all of the altered components, such as the main spring or stock snaps. Prototyping would allow for physical testing of the system. Ultimately, this proposal would be submitted to Nerf in order to implement the redesign.

REFERENCES

[1] "ABS." *Overview of materials for Acrylonitrile Butadiene Styrene (ABS), Molded*. Matweb. Retrieved from <http://www.matweb.com/search/DataSheet.aspx?MatGUID=eb7a78f5948d481c9493a67f0d089646> on April 15, 2010.